Validation of the Rain Profiling Algorithm "ZPHI" from the C-Band Polarimetric Weather Radar in Darwin

ERWAN LE BOUAR AND JACQUES TESTUD

Centre d'Étude des Environnements Terrestre et Planétaires, Velizy, France

TOM D. KEENAN

Bureau of Meteorology Research Centre, Melbourne, Australia

(Manuscript received 16 November 2000, in final form 28 February 2001)

ABSTRACT

An extensive application of a rain profiling algorithm (ZPHI) employing a C-band polarimetric radar (the C-POL radar of the Australian Bureau of Meteorology Research Centre in Darwin) is presented. ZPHI belongs to the class of rain profiling algorithms that have been developed for spaceborne or airborne radars operating at attenuating frequencies. By nature, these algorithms are nonlocal: the full profile of the measured radar reflectivity is inverted to derive a retrieved profile of the rainfall rate. The retrieval accuracy lays in the imposition of an "external constraint" in the inversion procedure. In this case, that is supplied by the differential phase shift Φ_{DP}. The primary products of ZPHI are the profile along the beam of the specific attenuation A, and the "normalized" intercept parameter N_0^*. The rainfall rate is further estimated through an R–A relation *adjusted for* N_0^*. ZPHI solves automatically two problems met when operating at C band: the along-path attenuation and the variability of the raindrop size distribution. Moreover, its robustness with respect to radar statistical error allows ZPHI to operate with short dwell times, important for operational applications.

To provide high quality rain-rate retrieval, ZPHI requires careful radar calibration. Two techniques of calibration checking are investigated; both provide a calibration estimate to within 0.1 and 0.2 dB. One is based upon the climatological stability of the N_0^* histogram. The second, which is purely radar based, uses a consistency test between the current rain-rate estimate by ZPHI and an estimate combining the specific attenuation A and the differential reflectivity Z_{DR}.

Comparisons of rain rate, including an extensive dataset in the month of January 1998, show a remarkable agreement between rain gauge data and the ZPHI estimate, whereas the "classical" estimate (standard Z–R relation applied without consideration of the attenuation) appears severely biased with respect to the rain gauges. In these comparisons, evidence for the crucial role of an N_0^* determination to improve the rain-rate estimate is provided.

1. Introduction

With the conventional weather radars deployed in most operational networks, the rainfall rate R is normally estimated from the radar reflectivity Z, using an empirical Z–R relation. These estimates are subject to large uncertainties, particularly because of the variability of the drop size distribution (DSD). Under the simple assumption that the DSD follows an exponential law of the form $N(D) = N_0 \exp(-3.67D/D_0)$ (where N is the concentration by drop size diameter D, N_0 is the intercept parameter, and D_0 is the "median volume" diameter), and with the hypothesis that the terminal fall velocity of raindrops V_t is described by a power law like $V_t \propto D^{0.67}$ (Atlas and Ulbrich 1977), one may establish Z–R relations of the form $Z \propto N_0^{-0.5} R^{1.5}$ or $Z \propto D_0^{2.33} R$, parameterized by N_0 and D_0, respectively. Since N_0 and D_0 are random variables subject to large fluctuations (Testud et al. 2001), none of these relations is able to predict R accurately from the knowledge of Z.

To overcome this problem, the anisotropy of the medium produced by the oblateness of raindrops has been exploited by polarimetric radars to provide new observables such as the differential reflectivity Z_{DR} and the specific differential phase shift K_{DP}. Using the quasi-functional relation existing between Z_{DR} and D_0, the above Z–R relation parameterized by D_0 may be transformed into a "two-parameter" estimator $R(Z, Z_{DR})$ much less dependent on the DSD variability (Chandrasekar et al. 1990; Gorgucci et al. 1995). Meanwhile the "quasi-linear" R–K_{DP} relationship found by Seliga et al. (1986), Sachidananda and Zrnić (1987), and Chandrasekar et al. (1990) enables an estimator $R(K_{DP})$ less

Corresponding author address: Dr. E. Le Bouar, Centre d'Étude des Environnements Terrestre et Planétaires, 10-12, Av. de l'Europe, 78140 Vélizy, France.
E-mail: erwan.lebouar@cetp.ipsl.fr

sensitive than $R(Z)$ to DSD variability. The combination of K_{DP} and Z_{DR}, first suggested by Jameson (1991) and further investigated by Gorgucci and Scarchilli (1997), provides a two-parameter estimator $R(K_{DP}, Z_{DR})$ also immune from DSD variability. These algorithms were designed primarily for S-band polarimetric radars and their application at C or X band is limited by two effects usually negligible at S band: (i) Z and Z_{DR} may be affected by a two-way path attenuation through the rain; and (ii) a backscattering effect, which may affect the measured differential phase shift Φ_{DP} (Keenan et al. 1997) and as a consequence may impact the accuracy of the subsequent K_{DP} determination. Another limitation of the above cited algorithms is the large number of independent samples required to obtain an estimate with an acceptable statistical uncertainty. This requires long radar dwell times, generally incompatible with typical operational applications.

The performance of any radar algorithm for rain-rate retrieval requires consideration of (i) the sensitivity of the estimate to the statistical variability of the radar signal, and (ii) the immunity of the estimator to the physical variability of the DSD. In the following, the uncertainties associated with each of these effects are denoted ''statistical uncertainty'' and ''physical uncertainty,'' respectively. Algorithm ZPHI developed by Testud et al. (2000) tends to combine the moderate statistical uncertainty of the classical $R(Z)$ estimate and the reduced physical uncertainty provided by the abovementioned polarimetric algorithms. ZPHI belongs to the class of rain profiling algorithms that have been developed for spaceborne or airborne radars operating at attenuating frequencies (Kozu et al. 1991; Iguchi and Meneghini 1994; Marzoug and Amayenc 1994; Testud and Oury 1997). By nature, these algorithms are nonlocal: the full profile of the measured radar reflectivity is inverted to derive a retrieved profile of the rainfall rate. The accuracy of the rain-rate retrieval is achieved by the application of an ''external constraint'' in the inversion procedure. In ZPHI, the external constraint is supplied by the differential phase shift $\Delta\Phi$ measured between the two range bounds r_1 and r_2 along the radial used to retrieve a rain rate profile. Three characteristics of algorithm ZPHI are important:

1) it may cope with a short radar dwell time;
2) it automatically performs a correction for attenuation (important at C and X bands); and
3) it determines, for each profile, a parameter N_0^* (''normalized'' intercept parameter of the DSD), which allows one to tune the rain relation.

These characteristics make ZPHI particularly suitable for operational applications, whatever the radar frequency (S, C, or X band). The potential capability of ZPHI has been investigated by Testud et al. (2000) using numerical simulations. The object of the present paper is to proceed to a validation of the algorithm with real data. For this purpose, ZPHI is applied to an extensive dataset from a polarimetric radar, and R and N_0^* retrievals are systematically compared with those derived from rain gauge and disdrometer. The radar data are provided by the C-POL radar (C band, polarimetric) of the Bureau of Meteorology Research Centre (BMRC), located near Darwin, Australia, and operated as a ground validation site of the Tropical Rainfall Measurement Mission (TRMM), described by Kummerow et al. (2000). After a brief description of ZPHI in section 2, an illustration of its application to the C-POL radar data is given in section 3. Two radar calibration techniques based upon ZPHI are then presented: the first one uses the climatology of N_0^* (section 4), the second, purely radar based, examines the consistency between the various polarimetric parameters, including Z_{DR} (section 5). Finally, section 6 presents a validation of the rain-rate retrieval by ZPHI, using the rain gauge network associated with the Darwin TRMM validation site.

2. ZPHI algorithm principle

a. Inverse model

The inverse model in algorithm ZPHI consists of a set of three relationships between A and Z_e, K_{DP} and A, and R and A, respectively [where A is the specific attenuation for horizontal (H) polarization, in dB km^{-1}; Z_e is the equivalent radar reflectivity for H polarization, in mm^6 m^{-3}; K_{DP} is the specific differential phase shift between H and vertical (V) polarization, in deg km^{-1}; and R is the rainfall rate in mm h^{-1}]. Each of these relationships is parameterized by N_0^* referred to, in the following, as the normalized intercept parameter of the DSD. Here N_0^* is defined as

$$N_0^* = \frac{4^4}{\pi\rho_w}\frac{\mathrm{LWC}}{D_m^4}, \tag{1}$$

where LWC is the liquid water content, ρ_w is the density of liquid water, and D_m is the ''mean volume diameter'' (ratio of the fourth to the third moment of the raindrop size distribution). Whatever the shape of the DSD, N_0^* represents the intercept parameter N_0 of the exponential distribution having the same LWC and D_m as the actual one (Testud et al. 2001).

It was shown in Testud et al. (2000) that, after normalization by N_0^*, quasi-universal relationships are established between any couple of integral parameters of the DSD (as A/N_0^* and Z_e/N_0^*, for example). Moreover, the relationships between A/N_0^* and Z_e/N_0^*, K_{DP}/N_0^* and A/N_0^*, R/N_0^* and A/N_0^*, respectively, as derived from T-matrix calculations, may be satisfactorily approximated by power laws, which leads to the following parametric representation of the ''inverse model'':

$$A/N_0^* = a(Z_e/N_0^*)^b \tag{2}$$

$$K_{DP}/N_0^* = \alpha(A/N_0^*)^\beta \tag{3}$$

$$R/N_0^* = p(A/N_0^*)^q, \tag{4}$$

TABLE 1. Rain relations used in this paper. The inverse model in algorithm ZPHI consists of relations 1, 2, and 3. The Z_{DR} correction and alternate rain estimator use 4 and 5. The relation used in the so-called classical estimate is 6 (in which N_0^* is fixed to 0.8 $e7$ m^{-4}).

	Relationship		$T = -4$°C	$T = 0$°C	$T = 5$°C	$T = 10$°C	$T = 15$°C	$T = 20$°C	$T = 25$°C
1	$A = aN_0^{*(1-b)}Z_e^b$	a	1.05 e−6	1.08 e−6	1.09 e−6	1.08 e−6	1.06 e−6	1.03 e−6	0.99 e−6
		b	0.754	0.768	0.785	0.798	0.810	0.820	0.828
2	$K_{DP} = \alpha N_0^{*(1-\beta)}A^\beta$	α	19.77	14.20	10.13	7.78	6.34	5.44	4.87
		β	1.055	1.033	1.009	0.990	0.974	0.960	0.950
3	$R = pN_0^{*(1-q)}A^q$	p	9.70	7.45	5.65	4.52	3.79	3.29	2.96
		q	0.828	0.810	0.791	0.776	0.762	0.751	0.742
4	$A_{DP} = mN_0^{*(1-n)}A^n$	m	33.75	33.24	33.87	35.61	38.14	41.37	45.18
		n	1.307	1.304	1.302	1.302	1.302	1.304	1.306
5	$R/A = eZ_{DR}^f$	e	391	443	515	595	683	778	877
		f	1.404	1.527	1.659	1.770	1.864	1.942	2.005
6	$R = sZ_e^t$	s	4.30 e−2	4.39 e−2	4.46 e−2	4.57 e−2	4.67 e−2	4.77 e−2	4.80 e−2
		t	0.624	0.622	0.621	0.619	0.617	0.615	0.614

where a, b, α, β, p, and q coefficients are functions of the temperature (T) only. These coefficients are calculated in the conditions hereafter specified.

A composite oblateness law for raindrop is considered: Keenan et al.'s (1997) law for equivalent drop diameter D between 0 and 1.3 mm, Andsager et al.'s (1999) law for D between 1.3 and 4.2 mm, and Bringi et al.'s (1982) law for $D > 4.2$ mm. Andsager et al.'s law is probably the best documented for intermediate drop diameter range, but it is not valid for $D > 4$ mm and it prescribes prolate shape for $D < 0.5$ mm. Bringi et al.'s (1982) law, which predicts an oblateness of raindrop very close to the equilibrium shape, seems the best consensus for drop diameters greater than 4.2 mm, a range where no measurement is available. However, in natural conditions where the large drops may oscillate, the mean shape may possibly deviate from equilibrium, as shown by Gorgucci et al. (2000), and this is one of the uncertainties of the inverse model.

The terminal fall velocity law is Lhermitte's (1988), which is the best model presently available.

The various coefficients of relationships (2), (3), and (4) are tabulated between −4° and 25°C in Table 1. With this inverse model, the impact of the DSD variability on relationships (2)–(4) is described by the ''equivalent'' intercept parameter N_0^* only. A verification of the pertinence of this model from a wide dataset of raindrop spectra can be found in Testud et al. (2001).

b. Algorithm ZPHI

Algorithm ZPHI operates as a ray-by-ray analysis. The primary radar observables considered in ZPHI are the apparent (attenuated) radar reflectivity Z_a, and differential phase shift Φ_{DP}. Here Z_a is related to the equivalent radar reflectivity Z_e through

$$Z_a(r) = Z_e(r) \exp\left[-0.46 \int_0^r A(s)\, ds\right], \tag{5}$$

where r is the radial distance from the radar.

In ZPHI, a segmentation along the beam is considered defined by the $n + 1$ bounds $\{r_0, r_1, \ldots, r_{n-1}, r_n\}$ (where $r_0 = 0$ and $r_n = r_{max}$, maximum range of the radar). Along each segment $[r_{i-1}, r_i]$, it is assumed that N_0^* is constant, which implies, according to (2), that A and Z_e are related through a power-law relationship. Thus, ZPHI is based upon a piecewise inversion of (5) based on Hitschfeld and Bordan's (1954) formulation. More specifically, within each segment $[r_{i-1}, r_i]$, the solution of (5) is written with respect to A in the following manner (Testud et al. 2000):

$$A(r) = \frac{A(r_i)Z_a^b(r)}{Z_a^b(r_i) + A(r_i)I(r, r_i)}, \tag{6}$$

where

$$I(r, r_i) = 0.46b \int_r^{r_i} Z_a^b(s)\, ds. \tag{7}$$

This expresses the profile of specific attenuation $A(r)$ along segment $[r_{i-1}, r_i]$, as a function of the profile of the observed Z_a, and of the value of A at the far bound r_i.

Meanwhile, the normalized intercept parameter $N_0^{*(i)}$ relevant to segment $[r_{i-1}, r_i]$ may be derived as (see Testud et al. 2000)

$$N_0^{*(i)} = \left[\frac{1}{a}\frac{A(r_i)}{Z_e^b(r_i)}\right]^{1/(1-b)} = \left[\frac{1}{a\zeta_{i-1}^b}\frac{A(r_i)}{Z_a^b(r_i) + A(r_i)I(r_{i-1}, r_i)}\right]^{1/(1-b)}, \tag{8}$$

with

$$\zeta_{i-1} = \exp\left[0.46 \int_0^{r_{i-1}} A(s)\, ds\right]. \tag{9}$$

With the above formulation, all the inversion problem is conditioned by the determination of the $A(r_i)$s, since subsequently $A(r)$, $Z_e(r)$, and the $N_0^{*(i)}$s may be derived using (6), (5), and (8). The determination of the $A(r_i)$s makes use of the measured differential phase shifts $\Delta\Phi^{(i)}$s defined as

$$\Delta\Phi^{(i)} = \Phi_{DP}(r_i) - \Phi_{DP}(r_{i-1}). \quad (10)$$

Assuming that the inversion has been processed to range r_{i-1}, the integration of (3) between r_{i-1} and r_i provides the following integral constraint:

$$\frac{\Delta\Phi^{(i)}}{2} = \alpha[N_0^{*(i)}]^{(1-\beta)} \int_{r_{i-1}}^{r_i} A^{\beta}(s)\, ds. \quad (11)$$

Equation (11) defines an implicit equation for the unknown $A(r_i)$ since $N_0^{*(i)}$ and $A(s)$ are function of $A(r_i)$ through (8) and (6), respectively. Note that when $\beta = 1$, the dependence on N_0^* vanishes in (11), and the integral on the right-hand side becomes merely the path attenuation between r_{i-1} and r_i. In this particular case, the solution $A(r_i)$ expresses simply as

$$A(r_i) = \frac{Z_a^b(r_i)\{\exp[0.23b\Delta\Phi^{(i)}/\alpha] - 1\}}{I(r_{i-1}, r_i)}. \quad (12)$$

In the general case where $\beta \neq 1$, an iterative numerical procedure is used to solve (11) for $A(r_i)$. However, since β remains very close to 1 whatever the temperature between $-4°$ and $+25°$C (see Table 1), the $A(r_i)$ given by (12) always constitutes a quite good ''first guess'' that allows one, when introduced as initial condition in the iterative procedure, to determine $A(r_i)$ in two or three iterations with a relative accuracy better than 10^{-5}.

It is worth noting that when $\beta = 1$, $A(r_i)$ given by (12) is *not* subject to the radar calibration error C [if Z_a is multiplied by C, $A(r_i)$ is unchanged]; nor is $A(r)$ given by (6). In the same condition N_0^* given by (8) *is* subject to the radar calibration (if Z_a is multiplied by C, N_0^* is multiplied by $C^{-b/(1-b)}$). When $\beta \neq 1$, the estimate of $A(r_i)$ resulting from the numerical solution of (11) depends on the radar calibration error, because of the presence of N_0^* in this equation. However, this dependence is quite weak since $(1 - \beta)$, the exponent of N_0^* in (11), is at most 0.05 for temperatures ranging from $-4°$ to 25°C.

The final step of algorithm ZPHI is estimating the rain rate R using (4). Thus the profile along the beam $R(r)$ is derived through an R–A relationship scaled by N_0^*.

c. Sensitivity of the rain-rate retrieval to measurement noise

For the purpose of an error analysis, it is sufficient to use the first-guess solution given by (12). From the $A(r)$ derived from (12), Testud et al. (2000) established that

$$\delta A(r)/A(r) \cong b\delta Z_a(r)/Z_a(r) + \delta(\Delta\Phi)/\Delta\Phi, \quad (13)$$

$$\delta N_0^*/N_0^* \simeq (1 - b)^{-1}\delta(\Delta\Phi)/\Delta\Phi, \quad (14)$$

$$\delta R(r)/R(r) \cong bq\delta Z_a(r)/Z_a(r) + (1 - qb)(1 - b)^{-1}\delta(\Delta\Phi)/\Delta\Phi. \quad (15)$$

Equation (13) shows that the relative error in $A(r)$ or in $R(r)$ is composed of an error random in space and time or ''speckle'' in Z_a (which is not correlated between any two range gates of the segment), and an error due to the uncertainty in $\Delta\Phi$ (which is the same for all range gates of the segment). For $N_i = 10$ independent samples and with $b \cong q \cong 0.8$, the relative error due to the speckle in Z_a is $\pm 25\%$ for $\delta A/A$ and $\pm 20\%$ for $\delta R/R$. The relative error due to $\Delta\Phi$ decreases as $1/\Delta\Phi$. It is $\varepsilon\sqrt{2}/\Delta\Phi$ for $\delta A/A$ and $(1 - qb)(1 - b)^{-1}\,\varepsilon\sqrt{2}/\Delta\Phi$ for $\delta R/R$, where ε is the standard error in Φ_{DP}. A typical value of ε for $N_i = 10$ is 2°. It is reasonable to require that the error in $\delta R/R$ due to $\Delta\Phi$ be less than or equal to 25%. This leads to $\Delta\Phi \geq 20°$. In order to relax this constraint, $\Delta\Phi$ is evaluated by averaging Φ_{DP} over 11 adjacent gates about each bound r_i [note that this averaging does not degrade the range resolution of $A(r)$ or $R(r)$, since $\Delta\Phi$ only acts as a global constraint at each segment]. After this 11 range gate averaging, the constraint becomes

$$\Delta\Phi \geq 6°. \quad (16)$$

When (16) is satisfied, the error in N_0^* is $\delta[\log_{10}(N_0^*)] \leq 0.30$. Thus the expected statistical error in N_0^* is ± 3 dB for $\Delta\Phi = 6°$, or ± 0.6 dB ($\pm 15\%$) for $\Delta\Phi = 30°$. Meanwhile, the expected total statistical error in R is $\pm 32\%$ when $\Delta\Phi = 6°$, and $\pm 21\%$ when $\Delta\Phi = 30°$.

When (16) is not fulfilled, it is considered that the full version of the algorithm collapses. Nevertheless, to get a retrieval, N_0^* is forced to the Marshall–Palmer (1948) value of $0.8\ 10^7\ \text{m}^{-4}$. In this case, $A(r_i)$ is derived from (8).

d. Partition scheme

A basic assumption in ZPHI is that N_0^* is constant along each segment $[r_{i-1}, r_i]$ of the partition. In reality, N_0^* is a highly variable parameter, subject to jumps (Waldvogel 1974) reflecting changes in the microphysical processes such as at the transition between ''stratiform'' and ''convective'' rain. From an extensive analysis of airborne microphysical data observed during the Tropical Ocean and Global Atmosphere Coupled Ocean–Atmosphere Response Experiment (TOGA COARE), described by Webster and Lukas (1992), Testud et al. (2001) confirmed the distinct behavior of N_0^* according to rain type, stratiform or convective. They showed that in the climatic zone of the west equatorial Pacific, N_0^* is, on average, $3 \times 10^6\ \text{m}^{-4}$ in stratiform rain, and $2 \times 10^7\ \text{m}^{-4}$ in convective rain. Large fluctuations in N_0^* were observed for both rain categories. However, this variability is essentially *from event to event*. Within one particular event after separating convective and stratiform rain, the variability of N_0^* is much more moderate.

Given the above, the partition scheme separately treats stratiform and convective rain. In convective rain, when several rain cells are encountered along the beam,

they are treated separately. That way, it is expected that the N_0^* variation along each segment will be minimized.

The partition scheme used herein is based upon the following approach.

1) At each ray, a first run is performed over the full profile of the available $\{Z_a(r), \Phi_{DP}(r)\}$, which allows retrieval of a first-guess $R_1(r)$.
2) A classification of the precipitation type along the beam is then undertaken using Testud et al.'s (2001) simple criterion. Namely, if $R_1(r) < R_{th}$ at the range r_0 and at adjacent ranges from $r_0 - \Delta r$ to $r_0 + \Delta r$, rain at range r_0 is classified as stratiform; otherwise it is convective. Here R_{th} is an arbitrary threshold and Δr represents the ''influence radius'' of a convective cell. In this paper R_{th} is taken to be 5 mm h^{-1} and Δr to 3 km.
3) Any convective segment defined by 2) is eventually resegmented if it includes more than one convective cell. The bounds of this new segmentation are chosen where $R_1(r)$ is minimum, but they do require that a minimum signal to noise ratio (>0 dB) be achieved in order to get a sufficient accuracy in the Φ_{DP} estimate. This new segmentation is retained only if it leads to $\Delta\Phi^{(i)}$s larger than 6°.
4) Within each of the segments thus defined, a second run of the algorithm is then undertaken according to the procedure outlined in section 2b. The inverse model [defined by (2), (3), and (4)] is tuned according to the temperature of the midpoint of the segment (estimated from its altitude).

It is important to note that the algorithm is quite robust with respect to the segmentation scheme. Its output is not sensitive to the values of the arbitrarily chosen parameters R_{th} and Δr.

e. *Correcting* Z_{DR} *for path attenuation: An alternate* R *estimate*

The differential reflectivity Z_{DR} is an interesting parameter that may be used to obtain an improved rain-rate estimate and, together with the other polarimetric parameters, to produce classification of hydrometeors (Vivekanandan et al. 1999). However, at C band, the along-path differential attenuation tends to induce a negative bias in Z_{DR} (because the horizontally polarized wave is more attenuated than the vertically polarized one). This negative bias may be quite severe after crossing a convective rain cell. Thus before any further use of Z_{DR} to improve a rain estimate or within a microphysical classification scheme, it is essential to correct it for differential attenuation. The ''true'' Z_{DR} may be expressed as a function of the ''apparent'' Z_{DRa}, observed by the radar, as

$$Z_{DR}(r) = Z_{DRa}(r) \exp\left[0.46 \int_0^r A_{DP}(s)\, ds\right], \quad (17)$$

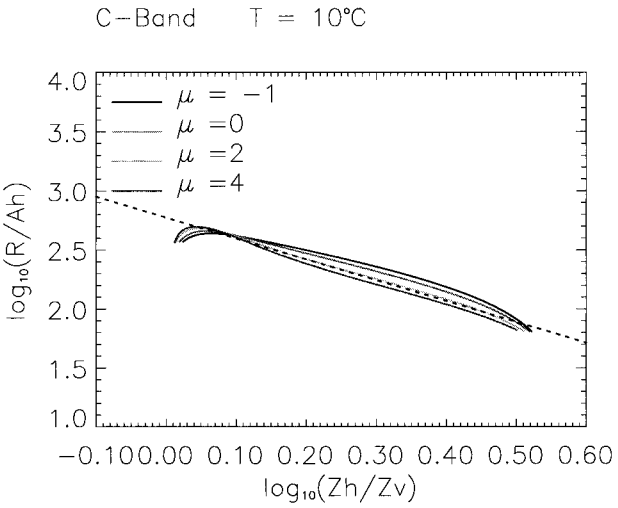

FIG. 1. R/A vs Z_{DR} at C band for four gamma drop size distributions as a function of the shape parameter μ. The dotted line represents the inverse model deduced from the gamma DSD with $\mu = 2$.

where A_{DP} is the specific differential attenuation between H and V in decibels per kilometer.

The inverse model (see Testud et al. 2000) also specifies the relation between A_{DP} and A (two integral parameters of the DSD) as

$$A_{DP}/N_0^* = c(A/N_0^*)^d. \quad (18)$$

Coefficients c and d are tabulated as a function of the temperature in Table 1. It should be noted that d is about 1.3 (thus the A_{DP}–A relationship does depend on N_0^*). After application of ZPHI, A_{DP} may be estimated at any range from the retrieved A and N_0^*, which helps one to calculate the integral in (17).

The same inverse model shows that the relation between two *intensive* variables is *independent of* N_0^* (and quasi-independent of the shape of the DSD). This is illustrated by the relation between Z_{DR} and δ (backscattering phase shift) shown in Testud et al. 2000. For the purpose of establishing an alternate estimate of the rain rate, Fig. 1 investigates the relation between R/A and Z_{DR} for different values of the shape parameter μ of the DSD. The dispersion between the various curves is quite moderate and the relationship appears linear (in log scales) from $Z_{DR} = 0.5$ to 5 dBZ. This leads to a model like

$$R/A = e(Z_{DR})^f, \quad (19)$$

which constitutes the alternate rain-rate estimate used in this paper.

Coefficients e and f are tabulated as a function of the temperature in Table 1 (assuming $\mu = 2$).

3. Illustration of ZPHI application to real data

ZPHI has been applied to one month of data (January 1998) collected by the C-POL polarimetric radar op-

TABLE 2. Specifications of the C-POL radar during the January 1998 TRMM validation experiment.

C-POL characteristics	
Antenna size	4.2 m
Beamwidth	1°
Radome	No
Wavelength	5.35 cm
Pulse width	1 μs
PRF	1000 Hz
Measured variables	Z_H, Z_{DR}, ρ_{HV}, Φ_{DR}, V_r, σ_v
Range resolution	300 m
Scanning strategy	Conical (17 elevations from 0.5° to 42.2°)
Azimuth sampling	1.45°
Doppler capability	Yes

erating near Darwin in Australia. Specific characteristics of this C-band radar are summarized in Table 2 (for more details, see Keenan et al. 1998). Most results presented hereafter were obtained after correcting the measured reflectivity by -1 dBZ, as a result of the recalibration procedures presented in section 5 and 6.

a. Illustration of ZPHI application to individual rays

As discussed in section 1, ZPHI operates on a ray-by-ray basis. Figure 2 illustrates its application to a particular ray at 1.6° elevation, where convective rain is sampled. At this elevation, the radar beam reaches 4.2-km altitude (center of the beam) or 5.2-km altitude (upper edge of the beam) at 120-km range, while the freezing level in January at Darwin is near 5-km altitude. Thus, except for the possible presence of hail in some convective cells, it is expected that rain is being sampled to 120-km range. From the profile along the radar beam of Z_a (thin line in Fig. 2a) and from the $\Delta\Phi$s associated with the segmentation of the Φ_{DP} profile (star symbols in Fig. 2c), the profiles of A and N_0^* at each segment are derived. Further, Z_e, resulting from the attenuation correction (heavy line in Fig. 2a) illustrates how significant along-path attenuation can be: at 118-km range, Z_a is underestimated by 15 dBZ with respect to Z_e.

In Fig. 2, the automated partitioning distinguishes three segments: (22 km, 44 km), (44 km, 82 km), and (82 km, 118 km). For the first, which is classified as being stratiform precipitation, $\Delta\Phi$ is below the threshold of 6°, hence N_0^* is fixed at the reference value of 0.8×10^7 m^{-4}. The other two (second and third) segments are classified as convective, and N_0^* is retrieved to be 1.58×10^7 m^{-4} and 10^7 m^{-4}, respectively.

The rainfall-rate profile $R(r)$ derived from the combination of $A(r)$ and N_0^* through (4) is shown in Fig. 2d, together with a ''classical estimate'' (derived as a result of the R–Z_e relationship with fixed N_0^*, defined in Table 1, applied to the ''apparent'' reflectivity Z_a without consideration of attenuation). At far range (third segment) it is seen that the rain-rate estimate by ZPHI is much higher than the classical estimate, and this is mainly due to the attenuation correction. But the ZPHI estimate is also much larger than the classical one for the rain cells of the second segment, which have undergone moderate integrated attenuation. This result is due to the tuning of the R–A relation by the retrieved N_0^*.

Figure 2b illustrates the ability of ZPHI to correct the observed Z_{DR} for attenuation. In this particular instance, the differential correction reaches 2 dB at far range. Such a correction is necessary for practical exploitation of Z_{DR} in rain-rate estimation or the classification of hydrometeors at C band. It is interesting to note that the corrected Z_{DR} profile is compatible with the presence of rain all along the profile (Z_{DR} ranging between $+1$ and $+4$ dB).

Fig. 3 shows that ZPHI operates properly in stratiform rain as well. Here the automated partitioning leads to two segments of 40-km length. In this case the integrated attenuation is much weaker (nevertheless reaching 3 dBZ at the far bound). But even with the correction for attenuation, the ZPHI retrieval leads to rainfall rates *smaller* than the classical estimate. This again is an effect of N_0^* tuning by ZPHI. For this particular ray, the retrieved N_0^* for both segments is 0.25×10^7 m^{-4}, much smaller than the Marshall–Palmer value prescribed in the classical estimate.

It should be emphasized that in the two rays illustrated in Figs. 2 and 3 (as in all rays processed by ZPHI in this paper), the dwell time (needed to collect 56 samples on both H and V polarization at 1000 Hz) is 112 ms.

b. Quality control

The inverse model, through (3), specifies the profile $K_{DP}(r)$ associated with $A(r)$ retrieved by ZPHI. Hence a ''theoretical'' profile of Φ_{DP} [denoted $\Phi_{DP}^{th}(r)$] may be derived along any integration path $[r_i, r_{i+1}]$ as

$$\Phi_{DP}^{th}(r) = \Phi_{DP}(r_i) + 2\int_{r_i}^{r} K_{DP}(s)\, ds = \Phi_{DP}(r_i) + 2\alpha \int_{r_i}^{r} N_0^{*1-\beta} A^{\beta}(s)\, ds. \quad (20)$$

It is important to recall that by construction, according to (11), $\Phi_{DP}^{th}(r_{i+1}) = \Phi_{DP}(r_{i+1})$ in (20). Thus $\Phi_{DP}^{th}(r)$ constitutes the optimal interpolation of Φ_{DP} between r_i and r_{i+1}, consistent with the profile of $Z_a(r)$.

In Figs. 2c and 3c, $\Phi_{DP}^{th}(r)$ (heavy line) is shown superimposed on $\Phi_{DP}(r)$ (thin line). This comparison enables one to objectively assess the $A(r)$ retrieval. Differences between theoretical and ''measured'' Φ_{DP} have five main sources: (i) statistical uncertainty (including thermal noise) in Φ_{DP}; (ii) bias in the Φ_{DP} measurement, due to antenna sidelobes; (iii) inadequacy of the inverse model due to the presence of hydrometeors other than rain; (iv) backscattering effect (δ) in the phase shift, affecting Φ_{DP} but not included in the model to derive

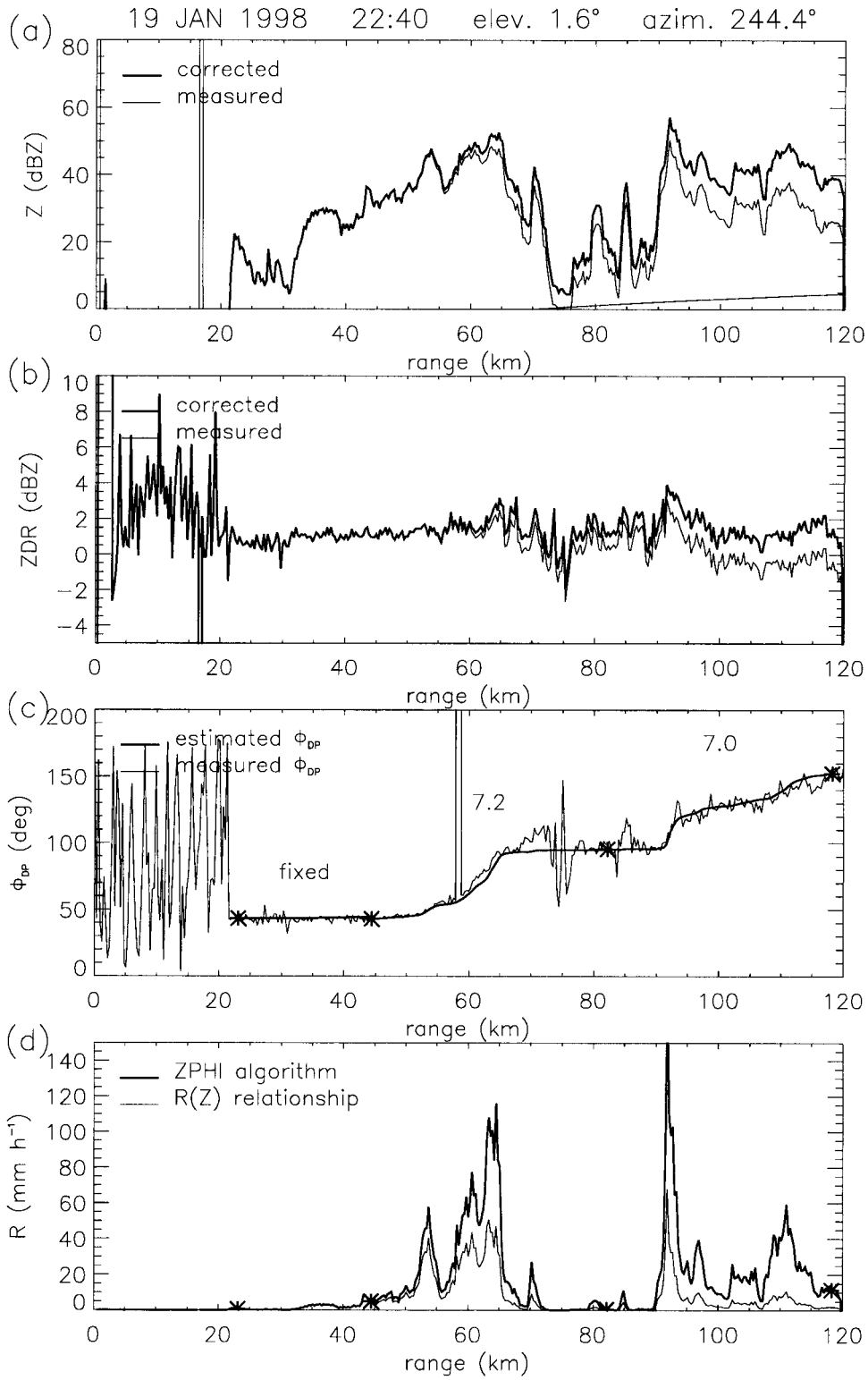

FIG. 2. For a convective rain case, profiles along the radar beam of (a) apparent measured reflectivity Z_a (thin line) and corrected equivalent reflectivity Z_e (heavy line); (b) measured differential reflectivity Z_{DRa} (thin line) and corrected one Z_{DR} (heavy line); (c) differential phase shift Φ_{DP}, measured (thin line) and model adjusted (heavy line); the numbers are $\log_{10}(N_0^*)$ and (*) symbols are boundaries of the ZPHI segmentation process; (d) retrieved rainfall rates from the classical estimate $R(Z_a)$ (thin line) and from ZPHI (heavy line). Vertical lines in (a) and (c) result from jumps caused by the acquisition process and are treated as spurious points in ZPHI.

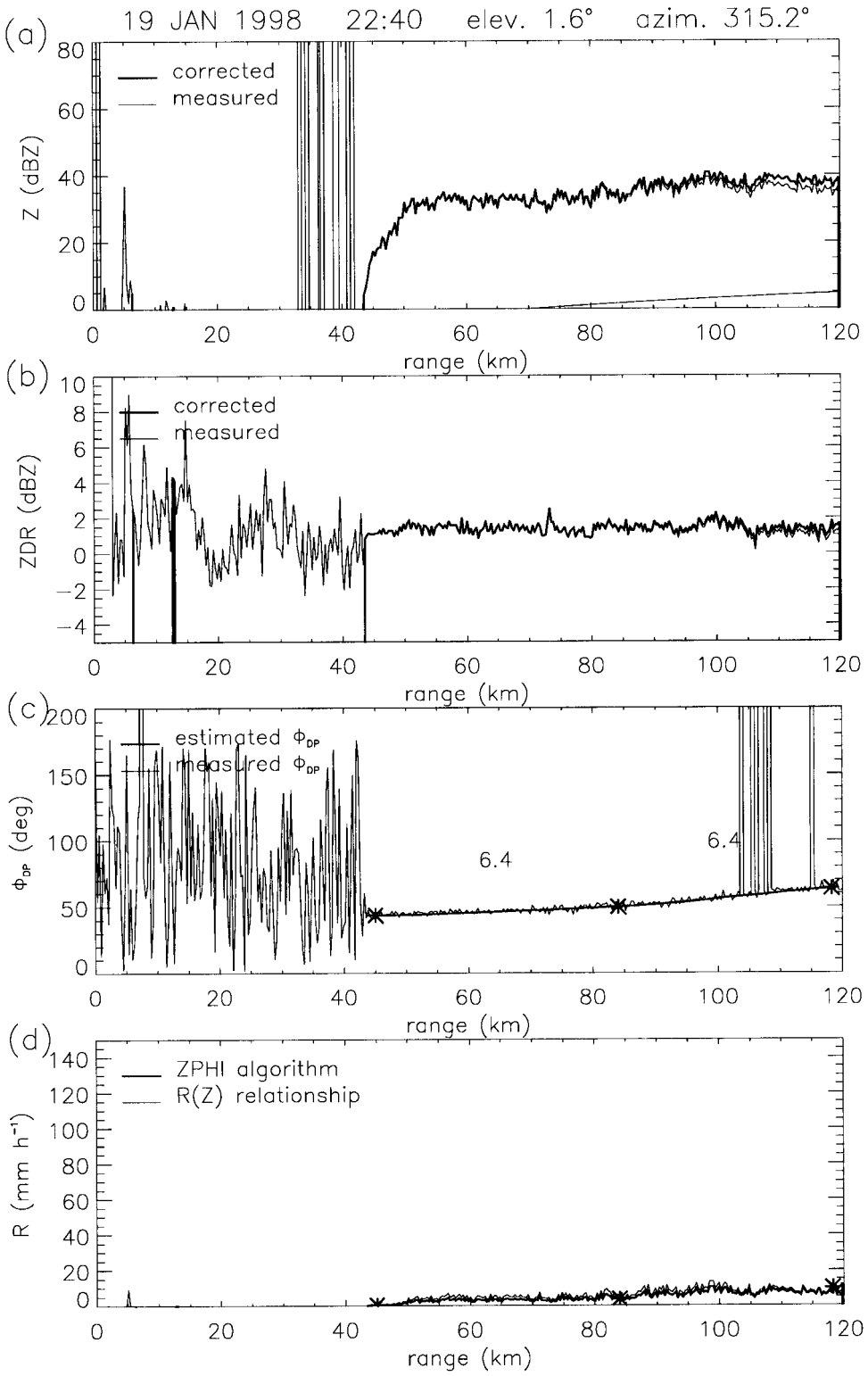

FIG. 3. As in Fig. 2 but for a stratiform case.

Φ_{DP}^{th}; and (v) inappropriate choice for the bounds of the segmentation.

Thermal noise in Φ_{DP} increases rapidly when the signal-to-noise ratio (SNR) gets below 0 dB, thus the quality control should be restricted to data points with SNR > 0 dB. Biases due to antenna sidelobes are expected in regions of sharp reflectivity gradients (as between 67- and 72-km range in Fig. 2). The contribution of δ to Φ_{DP} can be evaluated a posteriori thanks to the quasi-functional relationship between δ and Z_{DR} (see Testud et al. 2000): δ is negligible for $Z_{DR} < 1$ dB; $\delta \cong 1°$, 4.5°, and 9.5° for $Z_{DR} = 2$ dB, 3 dB, and 4 dB, respectively. An inappropriate choice of the segmentation bounds r_is induces inadequate estimates of the $\Delta\Phi_i$s, which impacts the full profile of Φ_{DP}^{th} (and, of course, that of A and R).

The segmentation is inappropriate when one (or several) of the r_is is set where the radar reflectivity Z_e is high (with a risk of significant backscattering phase shift), where Z_e is too low (predominance of thermal noise in Φ_{DP}), or where Z_e shows important gradients (risk of bias due to antenna side lobes). Our automated partition scheme is built to avoid such situations. Moreover, the fact that δ is negligible at any bound may be checked a posteriori by inspecting the retrieved Z_{DR}. If a bound is selected (as, for instance, the far bound) where δ is significant, it is always possible to solve the inversion problem in the iterative way described in Testud et al. (2000), that is, perform a first run of ZPHI ignoring δ, then calculate δ from Z_{DR}, then correct $\Delta\Phi$ for δ and use it in a next run of ZPHI, and so on. In practice, in this paper, the need for such a procedure never occurred.

A ''quality index,'' founded upon the calculation of the rms of $(\Phi_{DP}^{th} - \Phi_{DP})$ between r_i and r_{i+1} is established. If this rms value is less than 8°, the quality index is set to 1 for all points of the retrieved R profile. Otherwise it is set to zero.

An ''algorithm index'' also labels the retrieved R profile along each segment. It is set to 1 when R is derived from the full version of ZPHI (e.g., when $\Delta\Phi > 6°$), and to 0 otherwise (where the version of ZPHI with N_0^* forced to the Marshall–Palmer value is practiced).

c. *Comparison with a conventional* R–K_{DP} *approach*

The primary parameter retrieved by ZPHI is the specific attenuation A. Since A and K_{DP} are almost proportional, it could be argued that ZPHI is a new approach to retrieve K_{DP}. This new approach avoids Φ_{DP} differentiation, and by integrating the measured reflectivity profile in the process, it preserves the original range resolution of the radar and leads to a reduced statistical uncertainty. But the additional strength of ZPHI lays in the determination of N_0^*, which allows automatic tuning of the R–K_{DP} relation for the intrinsic DSD variability.

Figure 4 illustrates a full 360° conical scan (PPI) at 1.6° elevation, for which the product delivered by ZPHI is compared with that derived by the more conventional approach of May et al. (1999), consisting of deriving K_{DP} from Φ_{DP} and subsequently, estimating R from an R–K_{DP} relationship [referred to in the following as the $R(K_{DP})$ estimate]. May et al.'s (1999) method for estimating K_{DP} is based on a differentiation of Φ_{DP} after application of a nine-point filter, followed by a six-point consensus estimate procedure aiming to eliminate spurious effects introduced by occurrence of significant δ.

In Fig. 4, a stratiform rain structure is evident in the northwest quadrant, whereas a cluster of intense convective cells are observed in the southwest quadrant. Quite reasonable consistency is observed between the R retrievals of ZPHI (Fig. 4a) and the $R(K_{DP})$ estimate (Fig. 4c) in the convective cell cluster. In particular, heavy rain cells, which could be hidden by the attenuation effect, are evident away from the radar in both ZPHI and $R(K_{DP})$ retrievals. In contrast, in the stratiform area of the northwest quadrant, the difference between the two retrievals appears quite clear: while the $R(K_{DP})$ retrieval is very noisy, ZPHI produces a rain-rate field with a statistical error similar to that with the conventional $R(Z)$ estimate. Such a large statistical uncertainty with the $R(K_{DP})$ algorithm at low rain rate is not surprising. It represents the classical limitation of this type of algorithm.

The N_0^* product produced by ZPHI is illustrated in Fig. 4b. The gray areas are where N_0^* cannot be derived with sufficient accuracy (because $\Delta\Phi < 6°$) and ZPHI is run with N_0^* set to a fixed value (0.8×10^7 m^{-4}). In its full version including N_0^* retrieval, ZPHI operates over about 42% of the rainy area. But in terms of ''area-integrated rainfall,'' it captures a higher proportion of the rainfall (63%) because it treats preferentially the most intense rain areas. Where N_0^* is retrieved, Fig. 4b shows distinct N_0^* jumps between convective and stratiform (low values in stratiform, high values in convective) in agreement with the observations of Testud et al.'s (2001) obtained from the TOGA COARE airborne microphysical data.

The ray pattern in the rain field in the northwest quadrant of Fig. 4a (stratiform rain) is due to the statistical error in the retrieved N_0^*. According to (14), the relative error in N_0^* is proportional to the relative error in $\Delta\Phi$. Thus it may be quite significant in stratiform rain where $\Delta\Phi$ is small. The modeling error in R associated with an error in N_0^* is obviously correlated along each individual segment, which produces the ray pattern in question. The only way to improve the picture is to reduce the error in $\Delta\Phi$. This could be achieved by filtering Φ_{DP} across beam (in addition to the along-beam filtering already practiced).

4. Calibration check from N_0^* statistics

a. N_0^* *statistics at Darwin*

The precipitation regime at Darwin in January is usually tropical oceanic. The similarity of this precipitation with that observed during TOGA COARE is attested to

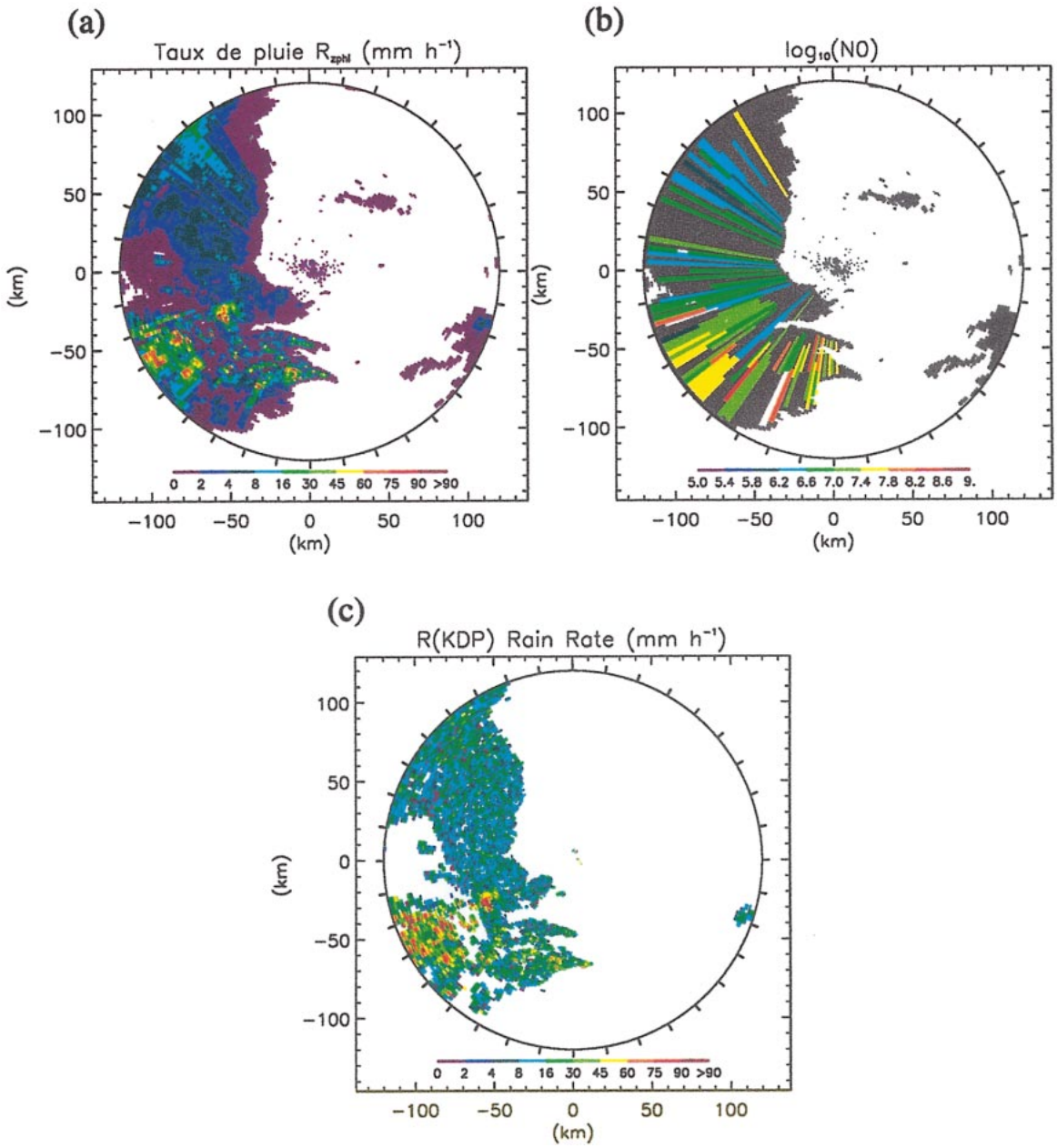

FIG. 4. Conical C-POL scan views (at 1.6° elevation, 19 Jan 1998 around 2240 UTC) of (a) the rainfall rate derived from ZPHI; (b) $\log_{10}(N_0^*)$ retrieved by ZPHI (in gray when forced to the Marshall–Palmer value); (c) the rainfall rate $R(K_{DP})$ derived from May et al.'s (1999) procedure.

by the strong resemblance between the N_0^* histogram observed by Dou et al. (1999) and that derived from the ground-based disdrometer from near Darwin (the Kowandi South BMRC station) during five rainy days of January 1998. Both histograms are bimodal, each mode corresponding to stratiform and convective rain, respectively (Fig. 5). The following describes how the stability of the N_0^* histogram may be utilized to fine-tune the radar calibration.

b. A calibration procedure founded upon N_0^*

The sensitivity of the N_0^* retrieval to the radar calibration error was already mentioned. A simple analysis of (8) shows that if C is the radar calibration error (in dBZ), then N_0^* is biased by a factor $10^{-[b/(1-b)]C/10}$. Thus, if one considers a histogram of $\log_{10}(N_0^*)$, derived from an extensive application of ZPHI on a large dataset, for a calibration error C, that histogram is expected to be

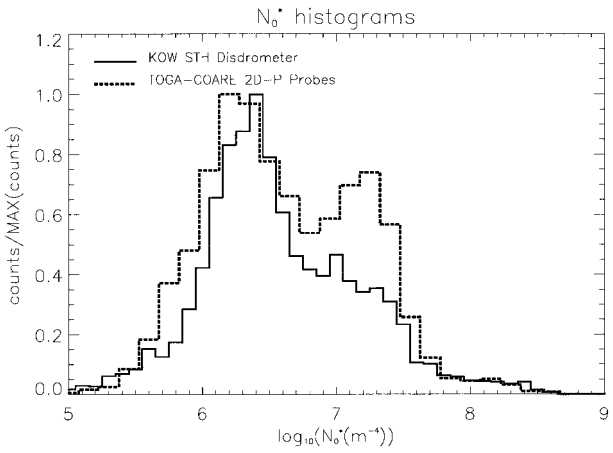

FIG. 5. Histograms of $\log_{10}(N_0^*)$ derived from the Kowandi South BMRC disdrometer for five days of Jan 1998 (full line), and from 2D-P probes during 21 flights of TOGA COARE (dotted line).

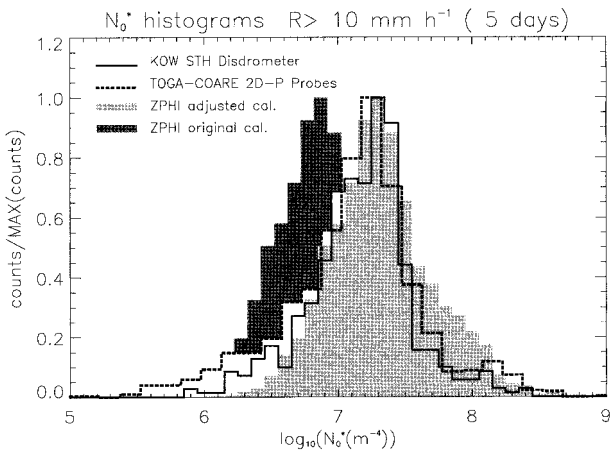

FIG. 6. Histograms of $\log_{10}(N_0^*)$ for rainfall rate greater than 10 mm h^{-1}, derived (i) from ZPHI (dark and light gray filled), (ii) from the Kowandi South BMRC disdrometer for five days of Jan 1998 (full line), and (iii) from 2D-P probes during TOGA COARE (dotted line). The light gray filled histogram is from ZPHI after a calibration adjustment in Z_a of -1 dBZ, while the dark gray filled one is for ZPHI with the original Z_as.

shifted by $-[b/(1-b)]C/10$ with respect to the actual one. For $C = 1$ dBZ and $b = 0.8$, the shift is 0.4. If one admits that the position of the peaks in the $\log_{10}(N_0^*)$ histogram is stable to ± 0.1 for a sufficiently large dataset, it is conceivable to adjust C to obtain Z_e within ± 0.25 dBZ accuracy.

However, the practical application of this method requires some caution. As specified in section 2b, the N_0^* retrieval by ZPHI is only applied for ray segments whose $\Delta\Phi$ is greater than 6°, which roughly represents a rain rate greater than 6.4 mm h^{-1} over 20 km or greater than 2.7 mm h^{-1} over 60 km. With such thresholds, it is expected that the statistics of the N_0^* histogram provided by ZPHI are biased for stratiform rain. Thus for meaningful comparison between N_0^* histograms derived from ZPHI and those observed from airborne microphysical probes or ground-based disdrometers, it is appropriate to select high rainfall rates only. A threshold $R > 10$ mm h^{-1} is presently considered, which practically selects only convective rain.

Figure 6 compares such histograms (with the threshold $R > 10$ mm h^{-1}) from three different data sources:

1) TOGA COARE airborne microphysical data (all flights);
2) Kowandi South disdrometer measurements, for five rainy days of January 1998; and
3) ZPHI outputs restricted to data falling within a 10-km radius centered at the disdrometer site (indicated in Fig. 8), for the same five days of January 1998.

The convective histograms from TOGA COARE (dashed line) and Kowandi South disdrometer (full line) are closely coincident, confirming the stability of the N_0^* statistics in a given precipitation regime. The general shape of the histogram derived from ZPHI (light gray) is consistent with the other two. However, to make the peak of the ZPHI histogram coincident with that of the ground-based disdrometer, an adjustment of the radar calibration by -1 dBZ is necessary. This leads one to consider that there is a residual calibration error C in the Darwin radar data of $+1$ dBZ. Otherwise the histogram provided by ZPHI (backward histogram in dark gray) is shifted leftward by -0.45 (in log scale). This technique of tuning the radar calibration by adjusting the peak of the N_0^* histogram derived by ZPHI to a reference (from ground truth or climatological) seems very accurate (probably to a few tenths of dB), while the limitation of any calibration procedure by hardware technique is about ± 1 dB.

5. Internal calibration check with ZPHI

The possibility of *internally* calibrating a dual polarization radar was previously investigated by Gorgucci et al. (1992) and Goddard et al. (1994). Gorgucci et al.'s approach is founded upon the examination of the consistency between two polarimetric rain-rate estimates (one using Z_H and Z_{DR}, the other K_{DP}), while Goddard et al.'s technique determines the radar calibration by checking directly the consistency between the three polarimetric variables Z_H, Z_{DR}, and Φ_{DP}. These techniques are certainly efficient at S-band where the path-integrated attenuation is negligible, but they cannot be used at C band without adaptation because of the attenuation affecting both Z_H and Z_{DR}.

The technique proposed in this section is connected to the previous approaches cited, but it takes advantage of the ability of ZPHI to correct Z_H and Z_{DR} for path attenuation. It is based on the principle that the two R estimates defined by (4) and (19) have different sensitivities to the radar calibration. Equation (4) provides the standard ZPHI estimate and is referred to in the following as R_{ZPHI}. This R_{ZPHI} combines A (parameter

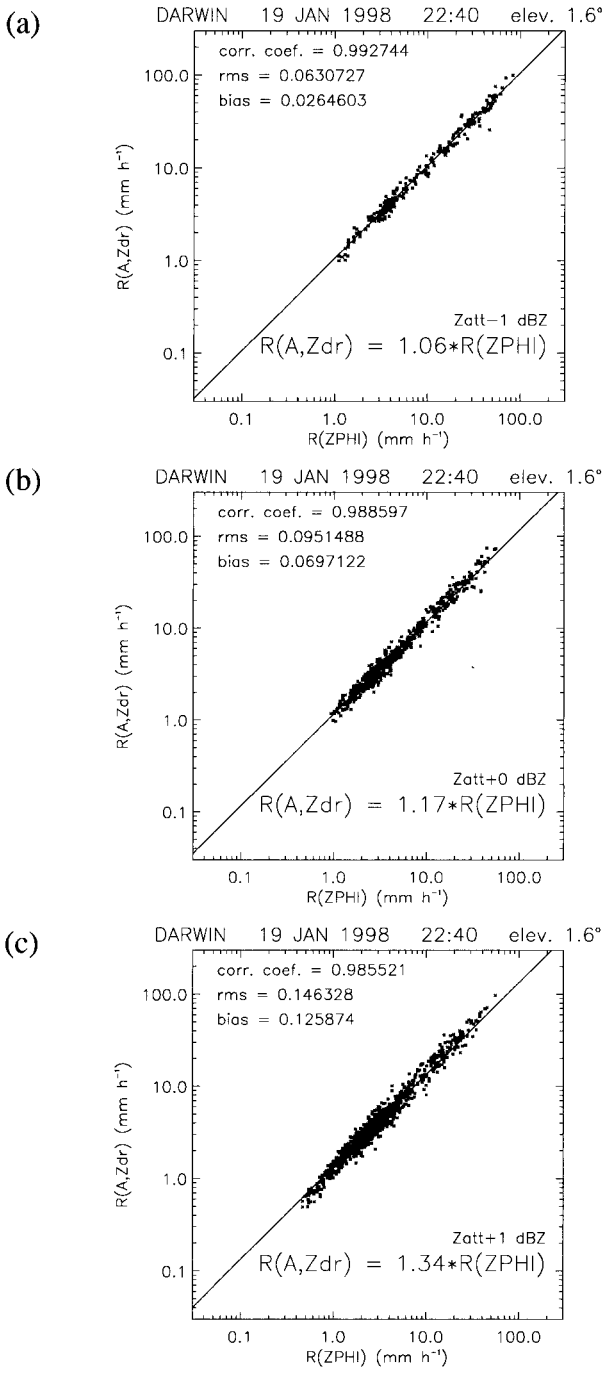

FIG. 7. Scatterplots of $R_{A,ZDR}$ against R_{ZPHI} for $r < 60$ km and $Z_{DR} > 1$ dB, after applying calibration corrections in Z_a of (a) −1 dB, (b) 0 dB, and (c) +1 dB.

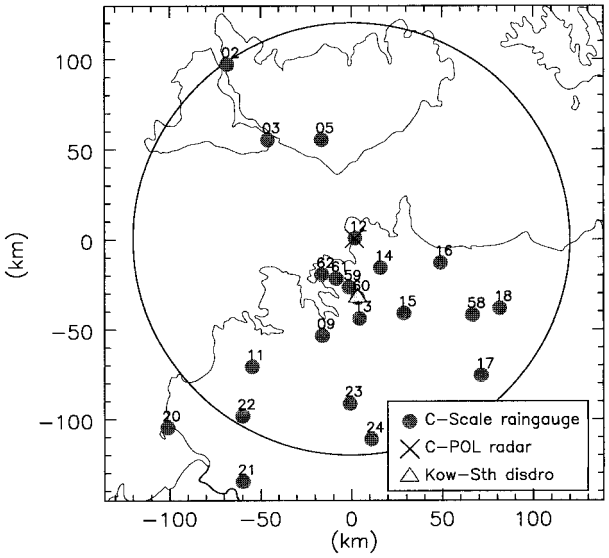

FIG. 8. C-scale rain gauge network spread around the C-POL radar, inside a 120-km-radius area. Position of the Kowandi South Disdrometer is also shown.

independent of the radar calibration error C) and N_0^* (dependent on C as $10^{-b/(1-b)\cdot C/10}$). The alternate estimate given by (19) combines A and Z_{DR} (referred to in the following as $R_{A\text{-}ZDR}$). If there were no attenuation, Z_{DR} would be independent of the radar calibration. But because of the differential attenuation, Z_{DR} depends on the calibration in a complex way due to the fact that A_{DP} in (18) depends on N_0^* as $\approx[N_0^*]^{-0.3}$ (see Table 1). Hence the path-integrated differential attenuation (in dB km^{-1}) that corrects Z_{DR} varies with the calibration error C as $\approx 10^{0.3b/(1-b)\cdot C/10}$. This represents quite a nonlinear dependence. If a short range ($r < 60$ km) is employed, the integrated differential attenuation is normally moderate, thus the sensitivity of $R_{A\text{-}ZDR}$ to radar calibration would be small. Then the dominant feature in the comparison between R_{ZPHI} and $R_{A\text{-}ZDR}$ is the R_{ZPHI} sensitivity to C. Figure 7 displays three scatterplots of R_{ZPHI} against $R_{A\text{-}ZDR}$ obtained for $r < 60$ km, $Z_{DR} > 1$ dB, and with three corrections to the radar calibration of −1 dB, 0 dB, +1 dB. In the three cases the scatterplot is well represented by a linear relationship (the linear correlation coefficient is higher than 0.985 in the three cases), but the best comparison is clearly obtained for the (−1 dB) correction, with a coefficient of proportionality between $R_{A\text{-}ZDR}$ and R_{ZPHI} of 1.06 (while it is 1.17 for 0 dB, and 1.34 for +1 dB) and a correlation coefficient of 0.993 (instead of 0.989 for 0 dB and 0.986 for +1 dB). This result brings independent confirmation that the residual calibration error of the Darwin radar data is +1 dB. Figure 7 also shows that the accuracy of this internal calibration technique is far better than ±1 dB (probably of the order of ±0.2 dB).

6. Validation of ZPHI from rain gauge data

This section describes and applies a procedure to compare rainfall rates retrieved by ZPHI and those observed by the tipping-bucket rain gauges within the so-called C-scale network at Darwin. This network consists of 25 rain gauges spread within a 150-km radius (see Fig. 8). The current radar operation of the C-POL con-

sists of volume scanning, 360° in azimuth, and from 0.5° to 42.2° elevation; the complete cycle requires 12 min. For this comparison exercise, we have considered the radar data at the second tilt angle only (elevation of 1.6°). It could be argued that the lowest tilt angle is more appropriate for comparison with rain gauges. Nevertheless, at 0.5°, the N_0^* retrieval may not be reliable, because of beam blockage effects (which do not affect the A retrieval but do affect the Z_e retrieval). As already mentioned in section 3, in January at Darwin, with a 1.6° elevation, the radar beam stays below the 0°C isotherm as long as the range is restricted to less than 120 km. With this restriction, 19 of the 25 rain gauges of the C-scale network are usable.

For the comparison, it is necessary to take into account the fundamentally different sampling characteristics of the weather radar and of the rain gauge network.

1) *Space and time resolution:* With a rain gauge, the collection area is very small, but the integration time is long (typically 1 min); with the radar, each measurement is quasi instantaneous (each sample is collected in 0.12 s), but the sampling volume is large (typically 0.1 km^3).
2) *Sampling strategy:* From the rain gauge network, the sampling is continuous in time, but discontinuous in space (typical spacing with the C-scale network is 20 km; see Fig. 8); from the radar the sampling is continuous in space but discontinuous in time (revisit time is 12 min).
3) *Representation:* The radar measures precipitation at altitude and the rain gauge on the ground; during its fall, the precipitation may drift horizontally with the wind; it may also partially evaporate in dry ambient air or enhance by collecting water from low-level clouds. This general problem of representativeness in the comparison between rain gauge and radar data was treated in depth by Kitchen and Blackhall (1992) and Anagnostou et al. (1999).

a. Comparison protocol

The comparison protocol considered presently is derived from that used by Willis (1999, personal communication) with the Florida Nexrad weather radar and neighboring rain gauges. It includes both spatial and temporal filtering.

At each rain gauge site, the radar-derived rainfall rate is averaged horizontally within a circle of 2-km radius. The distance of 2 km approximates the scale of the horizontal drift associated with precipitation falling from 1 km altitude under a wind of 10 m s^{-1}.

Temporal filtering is also employed to compensate for the difference between the radar revisit time (12 min), and the 1-min sampling rate of the rain gauge. Both measurements are smoothed over a window of 30 min according to the bell-shaped weighting function $W(t)$ illustrated in Fig. 9. This weighting function is an

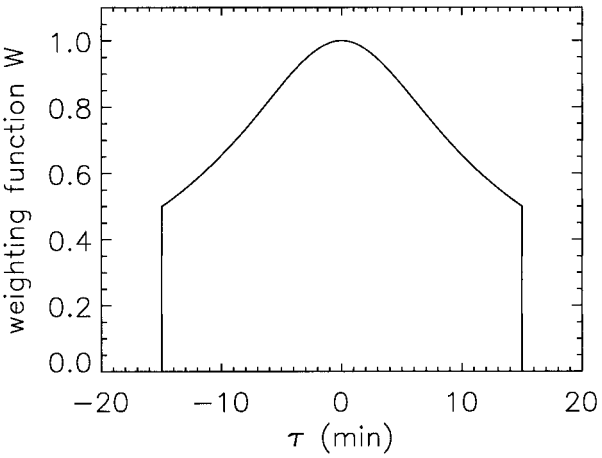

FIG. 9. Weighting function used in the time-averaging process to compare radar- and gauge-derived rain rates.

empirical approach to optimize the time averaging, taking account of the temporal correlation of the rain rate. More specifically, the ''filtered'' rain gauge estimate $\overline{G^{(i)}}$ by the ith rain gauge is calculated each minute as

$$\overline{G^{(i)}}(t) = \left[\sum_{t'=t-N_g\Delta t_g,\Delta t_g}^{t+N_g\Delta t_g} W(t'-t)G^{(i)}(t')\right] \times \left[\sum_{\tau=-N_g\Delta t_g,\Delta t_g}^{N_g\Delta t_g} W(\tau)\right]^{-1}, \quad (21)$$

where G_i is the 1-min estimate, $\Delta t_g = 1$ min, $N_g = 15$.

The filtered radar estimate is calculated every 12 min, at a time t centered at the averaged time of each 1.6° PPI sweep as

$$\overline{R^{(i)}}(t) = \left[\sum_{t'=t-N_r\Delta t_r,\Delta t_r}^{t+N_r\Delta t_r} W(t'-t)\langle R^{(i)}\rangle(t')\right] \times \left[\sum_{\tau=-N_r\Delta t_r,\Delta t_r}^{N_r\Delta t_r} W(\tau)\right]^{-1}, \quad (22)$$

where $\langle R^{(i)}\rangle$ is the spatial averaging of the radar estimate (within 2-km radius) at the ith rain gauge site, and $\Delta t_r = 12$ min, $N_r = 1$.

Three radar estimates are derived by the filtering defined by (22):

1) the ZPHI retrieval (corresponding filtered value is referred to as $\overline{R^{(i)}_{\text{ZPHI}}}$);
2) the result of the $R(A)$ relationship of Table 1, but at fixed Marshall–Palmer N_0^* (corresponding filtered value is referred to as $\overline{R^{(i)}_{\text{ATT.}}}$); and
3) the classical estimate (e.g., standard Z–R_e relationship applied to Z_a ignoring the along-path attenuation) (corresponding filtered value is referred to as $\overline{R^{(i)}_{\text{CLASS.}}}$).

As mentioned previously, the primary parameter re-

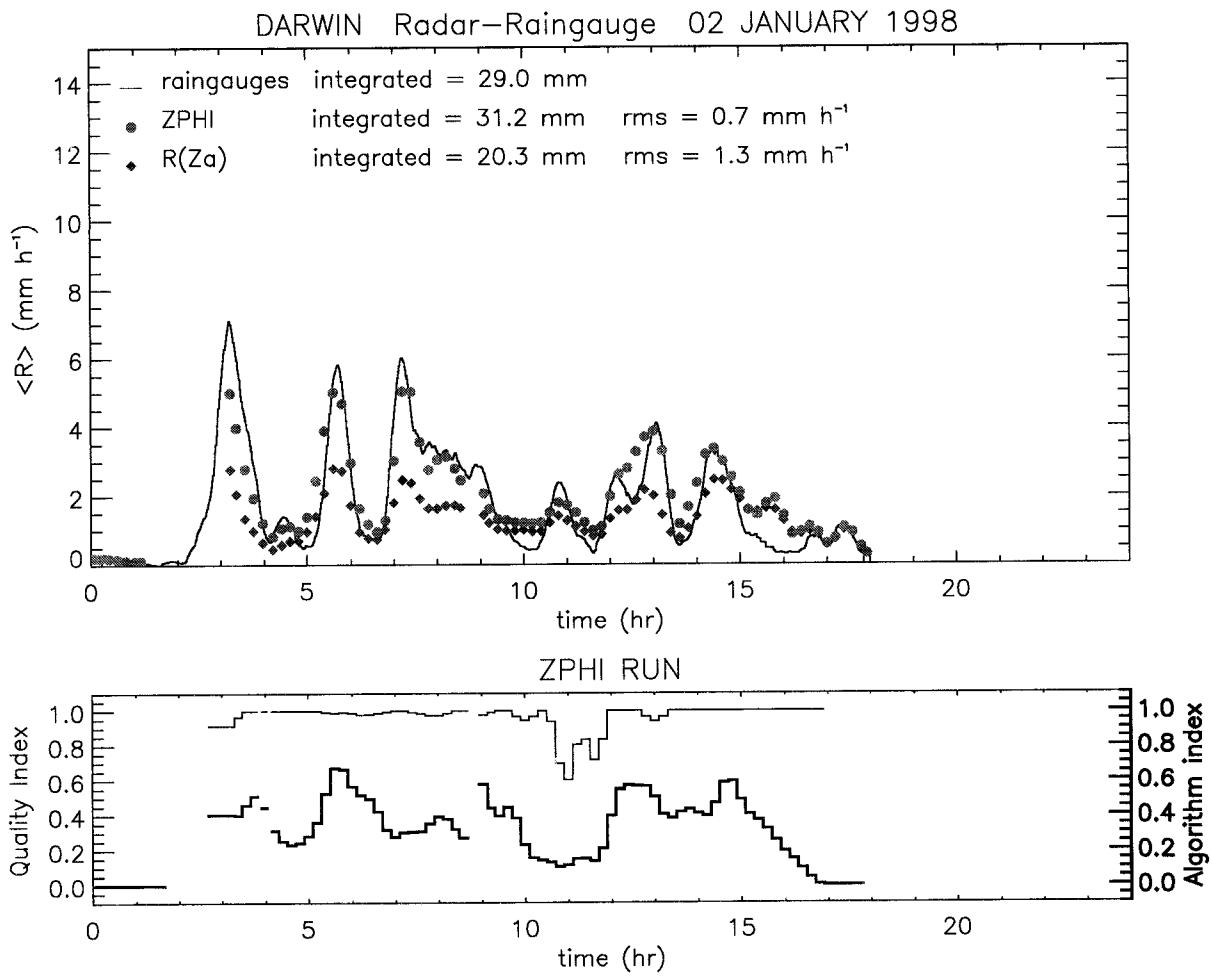

FIG. 10. Comparison of rain-rate time series on 2 Jan 1998. The rain rate, averaged over 19 rain gauge sites, is derived from rain gauge data (continuous line), and from radar data using the ZPHI algorithm (filled circle), or the classical estimate $R(Z_a)$ (filled diamond). The daily integrated rainfall rates are specified for each time series. The algorithm index (heavy line) and the ZPHI quality index (thin line) are also shown in the bottom panel for each radar-derived point of the time series.

trieved by ZPHI is the specific attenuation A. Since A and K_{DP} are almost proportional, $\overline{R^{(i)}_{ATT.}}$ may also be considered as the result of an $R(K_{DP})$ estimator with fixed N_0^*. The comparison of $\overline{R^{(i)}_{ATT.}}$ and $\overline{R^{(i)}_{ZPHI}}$ allows one to evaluate the improvement brought by *adjusting* N_0^* in the *R–A* relationship. It should be noted that with such a protocol, there is no mutual adjustment of the radar to the rain gauges. Both types of data are processed *independently*.

b. Comparison of time series

In this first series of comparison, we consider a fictitious watershed consisting of the assembly of the 19 circular catchments of 2-km radius centered at the rain gauge sites. The average rainfall rate in this watershed is denoted $G19(t)$ [average of the $\overline{G_i}(t)$s] when estimated from the rain gauge network, and $R19(t)$ [average of the $\overline{R_i}(t)$s] when estimated from the radar. Figures 10–12 illustrate the comparison of *G19* and *R19* time series during three days of January 1998 (2, 20, and 28 January). In each figure, two *R19* retrievals are shown: ZPHI (filled circle) and the classical estimate $R(Z_a)$ (filled diamond). In the bottom panel, the heavy-line time series labeled ''algorithm index'' is the 19-site average of the algorithm index (AI, defined in section 3b); it represents, as a function of time, the fraction of points where application of the full version of ZPHI (with retrieval of N_0^*) was met in the averaging process. Similarly, the thin-line time series labeled ''quality index'' is the 19-site average of the quality index QI (defined in section 3b). For instance, in Fig. 10 at 1000 UTC, an algorithm index of 0.25 means that 25% of the points used to obtain the average ZPHI estimate were processed with the full version of ZPHI. The corresponding quality index of, say, 0.9 means that, among the 25% points for which the full version of ZPHI applies, 90% have a quality index of 1.

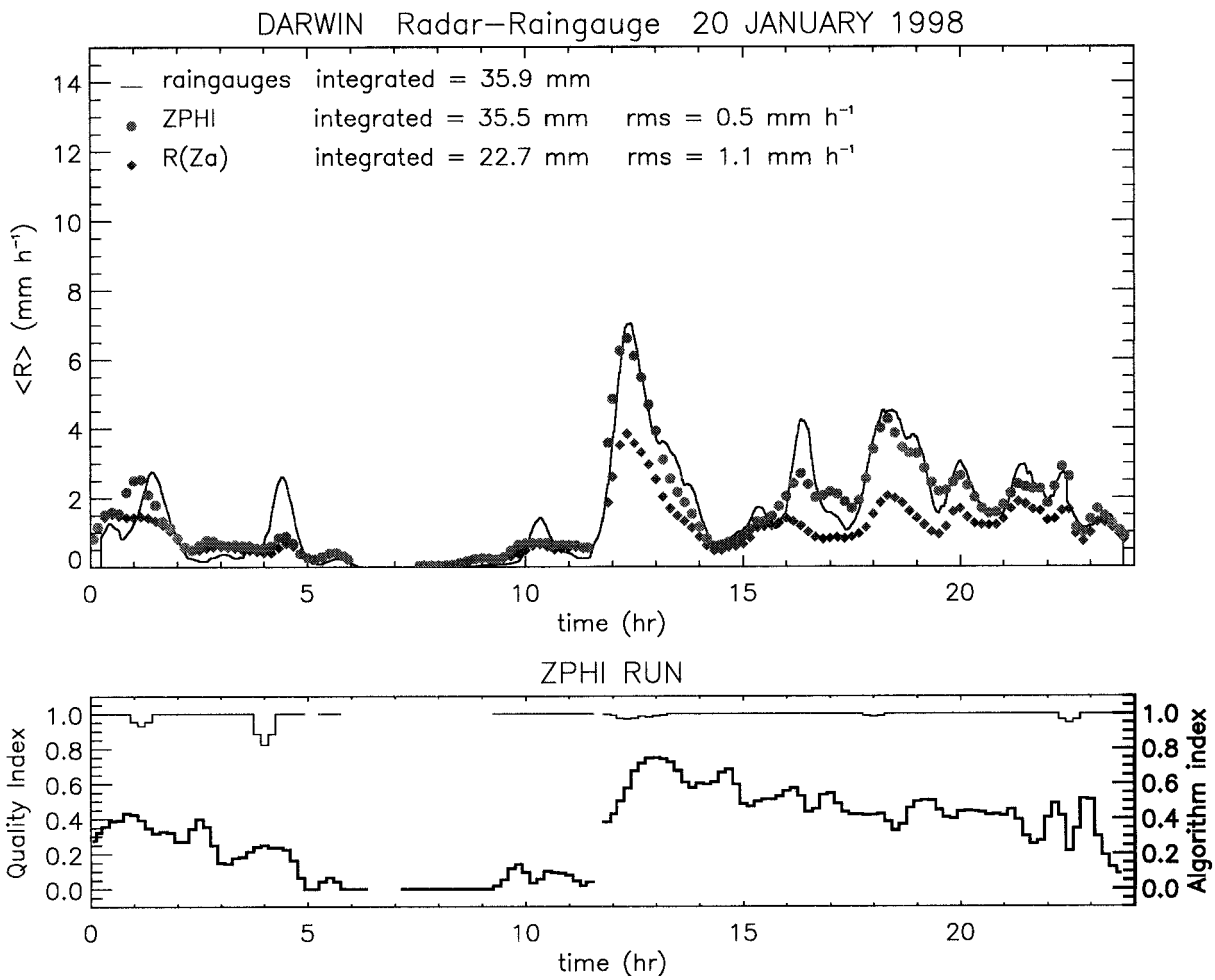

FIG. 11. As in Fig. 10 but for 20 Jan 1998.

A quick look through Figs. 10–12 shows that the ZPHI estimate follows remarkably well the estimate from the rain gauge network, while the classical estimate $R(Z_a)$ is unable to reproduce the peaks in *G19*, especially when their intensity exceeds 2 mm h^{-1}. This systematic underestimation of the classical estimate points out the importance of the ZPHI correction, and how precise its retrieval is, especially in case of heavy rain. The algorithm index indicates that the full version of ZPHI operates 40%–50% of the time on average, and more frequently in heavy rain rather than light rain (as expected). Most of the quality index is close to one. Local discrepancies between the *R19* estimate by ZPHI and *G19*, as observed in Fig. 10 around 1240 or 1540 UTC, are probably due to the representation error (as, e.g., that due to evaporation, making the rainfall rate measured at ground weaker than at altitude). It is also remarkable that the daily integrated rainfall obtained from ZPHI for the three days in question (31.2, 35.5, and 32.1 mm, respectively) is quite consistent with that calculated from rain gauge measurements (29, 35.9, and 34.3 mm), while the classical estimate $R(Z_a)$ leads to a severe underestimation (20.3, 22.7, and 18.5 mm).

c. *Point-by-point comparison*

Figure 13a is a scatterplot representing a point-by-point comparison between $\overline{R^{(i)}_{\mathrm{ZPHI}}}$ and $\overline{G^{(i)}}$, covering seven rainy days during January 1998 for the various available times and rain gauge sites. Figures 13b and 13c display a similar scatterplot but between $\overline{R^{(i)}_{\mathrm{ATT.}}}$ and $\overline{G^{(i)}}$, and between $\overline{R^{(i)}_{\mathrm{CLASS.}}}$ and $\overline{G^{(i)}}$, respectively. In these scatterplots, in order to isolate the improvement brought by algorithm ZPHI in its *full version* (i.e., with N_0^* retrieval), only data points where both ZPHI algorithm and quality indexes are 1 are retained. This corresponds to 41% of the total number of data points or 55% of the total area-integrated rainfall. Also, the comparison is restricted to data points within 60-km range in order to reduce the representation error between rain gauge and radar estimate.

Figure 13c confirms that the classical radar rain-rate

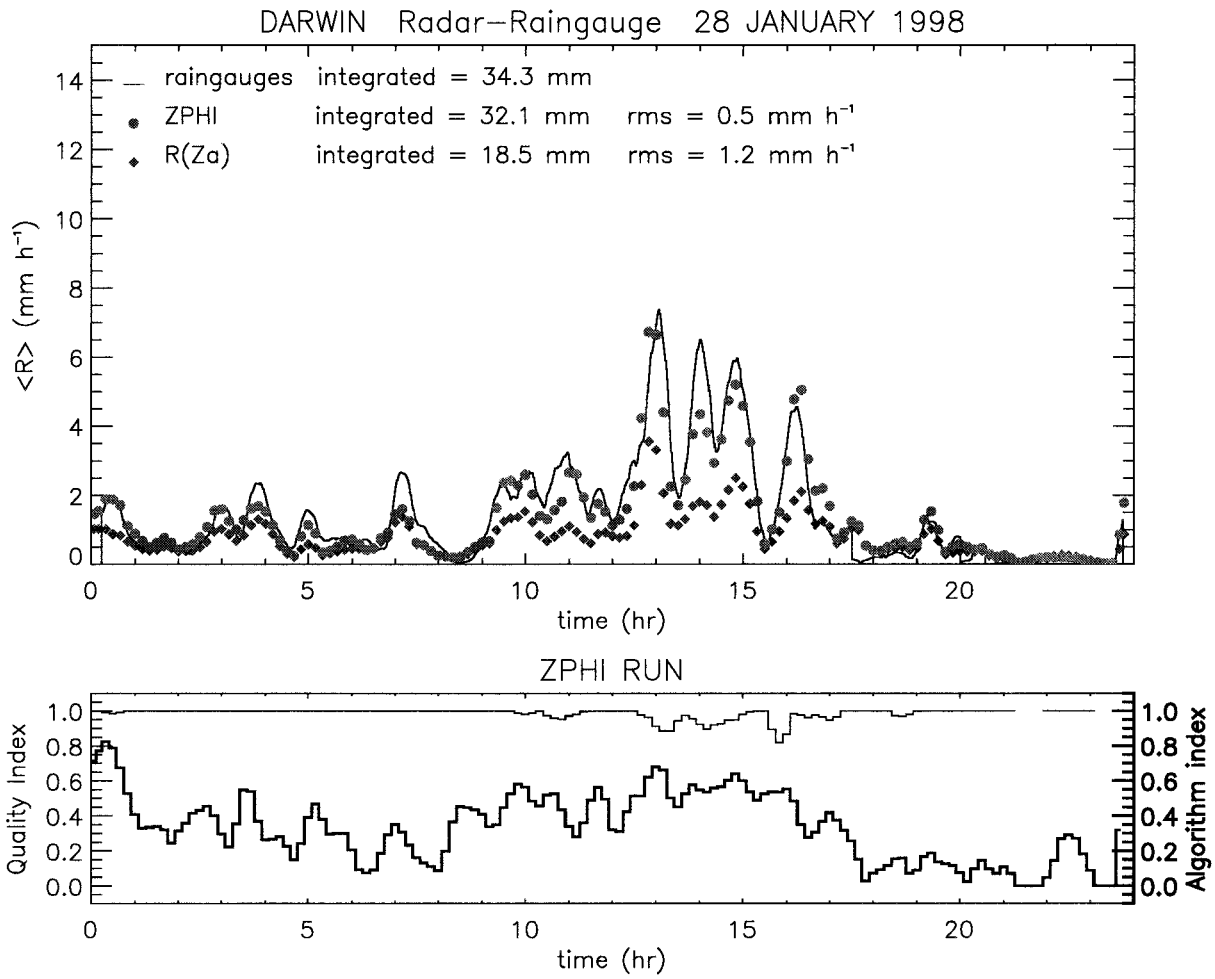

FIG. 12. As in Fig. 10 but for 28 Jan 1998.

estimate is severely biased with respect to the rain gauge: the slope of the linear fit is 0.37 (which means that, on average, the classical estimate $\overline{R^{(i)}_{\text{CLASS.}}}$ is only 37% of the gauge estimate $\overline{G^{(i)}}$). The use of the $R(A)$ estimate with fixed Marshall–Palmer N_0^* sensibly reduces the bias. The slope increases to 0.58, which is a serious improvement with respect to the classical estimate. With the ZPHI estimate [where the $R(A)$ relationship is tuned for the retrieved N_0^*] the slope jumps to 0.84. This demonstrates that not only the correction for attenuation, but also the N_0^* adjustment, is critical to retrieve good rainfall rate estimates at C band.

Another important statistical feature is the regular improvement of the ''linear correlation coefficient'' from Fig. 13c to Fig. 13a: $\rho = 0.871$ with the classical estimate; $\rho = 0.904$ with the $R(A)$ estimate with fixed N_0^*; $\rho = 0.918$ with ZPHI. This increase in ρ with $\overline{R^{(i)}_{\text{ATT.}}}$ and $\overline{R^{(i)}_{\text{ZPHI}}}$ should be interpreted as a reduction in the relative standard deviation (proportional to $\sqrt{1/\rho^2 - 1}$) with respect to the classical estimate ($\overline{R^{(i)}_{\text{CLASS.}}}$), of 20% and 30%, respectively.

When comparing rainfall rate estimates from rain gauge and radar, the bias and random errors are due to five effects:

1) the statistical error of the radar estimate;
2) the along-path attenuation (for $\overline{R^{(i)}_{\text{CLASS.}}}$ only);
3) the N_0^* variability (for $\overline{R^{(i)}_{\text{CLASS.}}}$ and $\overline{R^{(i)}_{\text{ATT.}}}$ estimates);
4) the representation error between rain gauge and radar; and
5) the rain gauge error.

The last two effects are the same for the three estimates. The statistical error of the radar estimate was theoretically analyzed in section 2c. It was shown that $\overline{R^{(i)}_{\text{CLASS.}}}$ is subject only to the speckle noise in Z_a, while $\overline{R^{(i)}_{\text{ATT.}}}$ and $\overline{R^{(i)}_{\text{ZPHI}}}$ are in addition subject to the statistical error in Φ_{DP}. The along-path attenuation acts as a bias (because it systematically leads to rain-rate underestimation) and as a noise source (because of its random character). The N_0^* variability acts to introduce ''noise,'' but it also introduces a bias because the intense rainfall rates have N_0^* values systematically higher than Marshall–Palmer value. The improvement of the correlation coefficient ρ mentioned above demonstrates that in spite

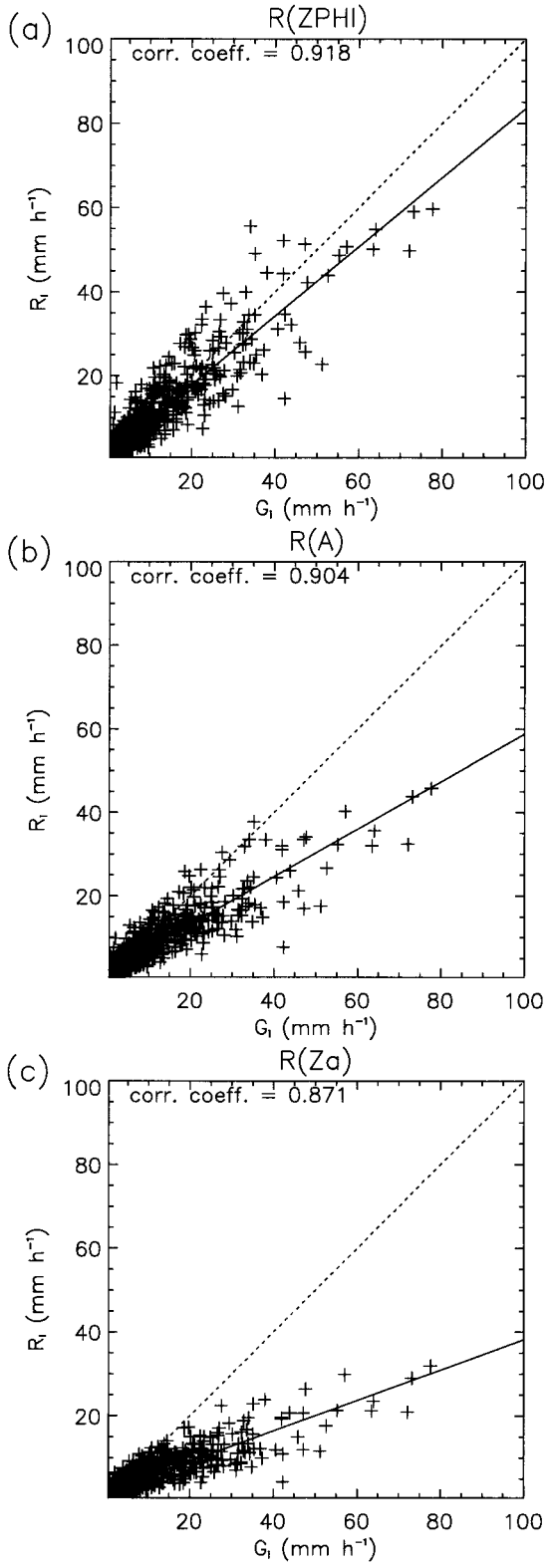

FIG. 13. Point-by-point comparison of gauge rainfall rate ($\overline{G^{(i)}}$ in the text) during seven days of Jan 1998, with collocated radar-derived estimates: (a) current ZPHI estimate ($\overline{R^{(i)}_{\mathrm{ZPHI}}}$ in the text), (b) *R–A* relation with fixed N_0^* ($\overline{R^{(i)}_{\mathrm{ATT.}}}$ in the text), (c) classical estimate R–Z_a ($\overline{R^{(i)}_{\mathrm{CLASS.}}}$ in the text).

of the increase in the statistical error due to their Φ_{DP} dependence, estimates $\overline{R^{(i)}_{\mathrm{ATT.}}}$ and $\overline{R^{(i)}_{\mathrm{ZPHI}}}$ bring finally a *reduction* of the total statistical error because they are corrected for along-path attenuation and for N_0^* variability (for $\overline{R^{(i)}_{\mathrm{ZPHI}}}$). According to Kitchen and Blackall (1992) and Anagnostou et al. (1999), the representativeness error of a rainfall estimate G by an individual rain gauge, with respect to the average rainfall A in a pixel of 3×3 km^2 or 4×4 km^2 (centered on the rain gauge), may be characterized by the variance of log(A/G). For hourly estimates, Kitchen and Blackall and Anagnostou et al. found that $\sigma^2[\log(A/G)] \cong 0.14$. The same characterization of the error may be considered in this paper using 30-min estimates $\overline{R^{(i)}}$ and $\overline{G^{(i)}}$. It is found that, for rain gauges at range smaller than 40 km from the radar:

$$\sigma^2\left\lfloor \log\left(\frac{\overline{R^{(i)}}}{\overline{G^{(i)}}}\right)\right\rfloor \cong 0.2 \quad \text{with the ZPHI estimate,}$$

and

$$\sigma^2\left\lfloor \log\left(\frac{\overline{R^{(i)}}}{\overline{G^{(i)}}}\right)\right\rfloor \cong 0.37 \quad \text{with the classical estimate.}$$

Thus ZPHI allows us to approach the variance of 0.14 associated with the representativeness error of the individual rain gauge, which should be considered as a ''theoretical limit'' that cannot be passed in such comparison exercise.

It is interesting to further comment on the difference between $\overline{R^{(i)}_{\mathrm{ATT.}}}$ and $\overline{R^{(i)}_{\mathrm{ZPHI}}}$. As mentioned previously, $\overline{R^{(i)}_{\mathrm{ATT.}}}$ is derived from the specific attenuation A and is representative of what would be obtained from an R–K_{DP} relationship since K_{DP} and A are nearly proportional. One could propose to adjust the coefficient of the *R–A* relation in order to obtain the same slope for the $\overline{R^{(i)}_{\mathrm{ATT.}}} - \overline{G^{(i)}}$ scatterplot as in the $\overline{R^{(i)}_{\mathrm{ZPHI}}} - \overline{G^{(i)}}$ approach. Such an adjustment would be equivalent to increasing N_0^* by a factor of 5 (with respect to Marshall and Palmer), which is statistically valid for high rain rates (corresponding to convective rain), but not for low rainfall rates observed in stratiform rain. Moreover, the only way to proceed with such an adjustment would be by comparison with a rain gauge network, while ZPHI operates the N_0^* adjustment ray by ray and segment by segment, without any reference to rain gauge.

7. Summary and conclusions

This paper presented an extensive application of algorithm ZPHI to the polarimetric data from the C-POL radar of BMRC, operating near Darwin, Australia. This should be considered as first results from real data, which need to be confirmed by a wider dataset. The primary data processed by ZPHI are the apparent (attenuated) reflectivity and the differential phase shift. The different steps in the rainfall-rate retrieval were discussed, showing the various capabilities of the algorithm, which include the following.

1) The segmentation of the analysis along each radar

beam, compensating for the basic hypothesis of ZPHI, that is, N_0^* constant along each segment.
2) The retrieval of the A profile (A: specific attenuation) and of parameter N_0^* characterizing the raindrop size distribution.
3) The retrieval of profiles of the equivalent radar reflectivity Z_e and differential reflectivity Z_{DR}, both corrected for effects of along-path attenuation.
4) The retrieval of the rainfall rate through an R–A relationship tuned for local value of N_0^*.

The mathematical simplicity of the algorithm, its robustness with respect to measurement noise, and its ability to check internally the quality of the retrieval make it particularly suitable in a real-time operational application. The main shortcomings of ZPHI seem to be presently the following.

1) ZPHI is based upon the hypothesis of constant N_0^* along the path. If N_0^* is not constant (which probably occurs along a path in stratiform rain), ZPHI adjusts an averaged N_0^*. Thus there may be a modeling error related to local deviation of N_0^* with respect to the adjusted average.
2) The inverse model of ZPHI depends on the oblateness law for raindrops. Some uncertainty remains about the averaged shape of large drops (with diameter greater than 4 mm), assumed close to equilibrium in this paper, but that may differ from equilibrium in natural conditions, due to drop oscillations.
3) When hail is met along the beam, the inverse model (designed for rain) is not appropriate. The hail region has to be identified and treated selectively, according to a process that remains to be specified.

The question of the radar calibration should be addressed carefully to get high quality products with ZPHI. In this paper two calibration techniques were investigated: one is founded upon the climatological stability of the N_0^* histogram; the second, purely internal to the radar, consists of a consistency test between the current rain rate estimated by ZPHI and an estimate obtained by combining A and Z_{DR}. Both techniques are very simple, provide a calibration estimate within 0.1–0.2 dB, and diagnose a consistent calibration error of -1 dB for the C-POL data of January 1998. The C-scale rain gauge network neighboring the Darwin radar was used to proceed to a systematic validation of the rain rates produced by ZPHI. Spatial and temporal filtering were applied to both data types in order to compensate for the quite different sampling characteristics of the radar and the rain gauges. A fictitious catchment consisting of an assembly of nineteen 2-km-radius circles, centered on the rain gauge sites, was first considered. Comparing time series of the average rain rate on this fictitious catchment, remarkable agreement was found between the rain gauge and the ZPHI estimate, while the classical estimate (standard Z–R relationship applied without consideration of the attenuation) appeared unable to represent properly the rainfall rate peaks. A point-by-point comparison was also performed including all available data from the month of January 1998. It confirmed that the classical estimate is severely biased with respect to the rain gauges (slope of linear correlation is 0.37). The estimate based upon A only (at fixed N_0^*) improves the comparison but the bias remains important (slope of linear correlation is 0.58). The ZPHI estimate (founded upon A *and* N_0^*) approaches best the rain gauge estimate with a slope of 0.84.

The A profile derived by ZPHI is also representative of a K_{DP} profile, since K_{DP} and A are nearly proportional. As compared to a conventional K_{DP} algorithm, ZPHI presents two advantages:

1) it allows derivation of the A profile with much less statistical error than that available with K_{DP} profile derived from conventional Φ_{DP} differentiation; and
2) it improves the bias and standard deviation of the rain-rate estimate by N_0^* tuning ray by ray, and segment by segment.

The Z_e and Z_{DR} retrievals are by-products of ZPHI that warrant particular interest. In combination with K_{DP} (derived from A) and the correlation coefficient ρ_{HV}, they may be used in a classification of the hydrometeors as performed by Keenan (1999) with the Darwin radar data.

Acknowledgments. This study was conducted in the framework of a contract between Météo-France and the Centre National de la Recherche Scientifique (CNRS). We acknowledge TSDIS of the TRMM office for providing the Darwin radar data and rain gauge data.

REFERENCES

Anagnostou, E. N., W. F. Krajewski, and J. Smith, 1999: Uncertainty quantification of mean-areal radar-rainfall estimates. *J. Atmos. Oceanic Technol.,* **16,** 206–215.

Andsager, K., K. V. Beard, and N. F. Laird, 1999: Laboratory measurements of axis ratios for large raindrops. *J. Atmos. Sci.,* **56,** 2673–2683.

Atlas, D., and C. W. Ulbrich, 1977: Path- and area-integrated rainfall measurement by microwave attenuation in the 1–3 cm band. *J. Appl. Meteor.,* **16,** 1322–1331.

Bringi, V. N., J. W. F. Goddard, and S. M. Cherry, 1982: Comparison of dual polarization radar measurements of rain with ground based disdrometer measurements. *J. Appl. Meteor.,* **21,** 252–264.

Chandrasekar, V., V. N. Bringi, N. Balakrishnan, and D. S. Zrnic, 1990: Error structure of multiparameter radar and surface measurements of rainfall. Part III: Specific differential phase. *J. Atmos. Oceanic Technol.,* **7,** 621–629.

Dou, X., J. Testud, P. Amayenc, and R. Black, 1999: The concept of normalized gamma distribution to describe raindrop spectra, and its use to parameterize rain relations. Preprints, *29th Conf. on Radar Meteorology*, Montreal, PQ, Canada, Amer. Meteor. Soc., 625–628.

Goddard, J. W. F., J. Tan, and M. Thurai, 1994: Technique for calibration of meteorological radars using differential phase. *Electron. Lett.,* **30,** 166–167.

Gorgucci, E., and G. Scarchilli, 1997: Intercomparison of multipa-

rameter radar algorithms for estimating rainfall rate. Preprints, *28th Conf. on Radar Meteorology*, Austin, TX, Amer. Meteor. Soc., 55–56.

——, ——, and V. Chandrasekar, 1992: Calibration of radars using polarimetric techniques. *IEEE Trans. Geosci. Remote Sens.,* **30,** 853–858.

——, ——, and ——, 1995: Radar and surface measurements of rainfall during CaPE: 26 July 1991 case study. *J. Appl. Meteor.*, **34,** 1570–1577.

——, ——, and ——, 2000: Measurements of mean raindrop shape from polarimetric radar observations. *J. Atmos. Sci.,* **57,** 3406–3413.

Hitschfeld, W., and J. Bordan, 1954: Errors inherent in the radar measurement of rainfall at attenuating wavelengths. *J. Meteor.*, **11,** 58–67.

Iguchi, T., and R. Meneghini, 1994: Intercomparison of single frequency methods for retrieving a vertical rain profile from airborne or space borne data. *J. Atmos. Oceanic Technol.,* **11,** 1507–1516.

Jameson, A. R., 1991: A comparison of microwave techniques for measuring rainfall. *J. Appl. Meteor.,* **30,** 32–54.

Keenan, T. D., 1999: Hydrometeor classification with a C-band polarimetric radar. Preprints, *29th Conf. on Radar Meteorology*, Montreal, PQ, Canada, Amer. Meteor. Soc., 184–187.

——, D. S. Zrnić, L. Carey, P. May, and S. Rutledge, 1997: Sensitivity of C-band polarimetric variables to propagation and backscatter effects in rain. Preprints, *28th Conf. on Radar Meteorology*, Austin, TX, Amer. Meteor. Soc., 13–14.

——, K. Glasson, F. Cummings, T. S. Bird, J. Keeler, and J. Lutz, 1998: The BMRC/NCAR C-band polarimetric (C-POL) radar system. *J. Atmos. Oceanic Technol.,* **15,** 871–886.

Kitchen, M., and R. M. Blackall, 1992: Representativeness errors in comparisons between radar and gauge measurements of rainfall. *J. Hydrol.,* **134,** 13–33.

Kozu, T., K. Nakamura, R. Meneghini, and W. Boncyck, 1991: Dual parameter measurement from space: A test result from an aircraft experiment. *IEEE Trans. Geosci. Remote Sens.,* **29,** 690–703.

Kummerow, C., and Coauthors, 2000: The status of the Tropical Rainfall Measurement Mission (TRMM) after two years in orbit. *J. Appl. Meteor.,* **39,** 1965–1982.

Lhermitte, R., 1988: Cloud and precipitation sensing at 94 GHz. *IEEE Trans. Geosci. Remote Sens.,* **26,** 207–216.

Marshall, J. S., and W. M. K. Palmer, 1948: The distribution of raindrops with size. *J. Meteor.,* **5,** 165–166.

Marzoug, M., and P. Amayenc, 1994: A class of single and dual frequency algorithms for rain rate profiling from a spaceborne radar. *J. Atmos. Oceanic Technol.,* **11,** 1480–1506.

May, P. T., T. D. Keenan, D. S. Zrnić, L. D. Carey, and S. A. Rutledge, 1999: Polarimetric radar measurements of tropical rain at a 5-cm wavelength. *J. Appl. Meteor.,* **38,** 750–765.

Sachidananda, M., and D. S. Zrnic, 1987: Rain rate estimates from differential polarization measurements. *J. Atmos. Oceanic Technol.,* **4,** 588–598.

Seliga, T. A., K. Aydin, and H. Direskeneli, 1986: Disdrometer measurements during an intense rainfall event in central Illinois: Implications for differential reflectivity radar observations. *J. Climate Appl. Meteor.,* **25,** 835–846.

Testud, J., and S. Oury, 1997: Algorithme de correction d' atténuation pour radar météorologique. *C. R. Acad. Sci. Paris,* **t324** (série 2a), 705–710.

——, E. Le Bouar, E. Obligis, and M. Ali-Mehenni, 2000: The rain profiling algorithm applied to polarimetric weather radar. *J. Atmos. Oceanic Technol.,* **17,** 332–356.

——, S. Oury, R. A. Black, P. Amayenc, and X. Dou, 2001: The concept of ''normalized'' distribution to describe raindrop spectra: A tool for cloud physics and cloud remote sensing. *J. Appl. Meteor.,* **40,** 1118–1140.

Vivekanandan, J., D. S. Zrnic, S. M. Ellis, R. Oye, A. V. Ryzhkov, and J. Straka, 1999: Cloud physics retrieval using S-band dual-polarization radar measurements. *Bull. Amer. Meteor. Soc.,* **80,** 381–388.

Waldvogel, A., 1974: The N_0 jump of raindrop spectra. *J. Atmos. Sci.,* **31,** 1067–1078.

Webster, P., and R. Lukas, 1992: TOGA COARE, The Coupled Ocean–Atmosphere Response Experiment. *Bull. Amer. Meteor. Soc.,* **73,** 1377–1416.